Manuscript accepted in Physics of Fluids, May 2017

Wall shear stress fluctuations: mixed scaling and their effects on velocity fluctuations in a turbulent boundary layer

Carlos Diaz Daniel,* Sylvain Laizet,† and J. Christos Vassilicos‡

Department of Aeronautics, Imperial College London, London, United Kingdom

Abstract

The present work investigates numerically the statistics of the wall-shear stress fluctuations in a turbulent boundary layer (TBL) and their relation to the velocity fluctuations outside of the near-wall region. The flow data is obtained from a Direct Numerical Simulation (DNS) of a zero pressure-gradient TBL using the high-order flow solver Incompact3D [S. Laizet and E. Lamballais, *J. Comput. Phys.*, 228, 5989 (2009)]. The maximum Reynolds number of the simulation is $Re_\theta \approx 2000$, based on the free-stream velocity and the momentum thickness of the boundary layer. The simulation data suggest that the root mean-squared fluctuations of the streamwise and spanwise wall shear-stress components τ_x and τ_z follow a logarithmic dependence on the Reynolds number, consistent with the empirical correlation of R. Örlü and P. Schlatter, *Phys. Fluids*, 23, 021704 (2011). These functional dependencies can be used to estimate the Reynolds number dependence of the wall turbulence dissipation rate, in good agreement with reference DNS data. Our results suggest that the rare negative events of τ_x can be associated with extreme values of τ_z and are related to the presence of coherent structures in the buffer layer, mainly quasi-streamwise vortices. We also develop a theoretical model, based on a generalisation of the the Townsend-Perry hypothesis of wall-attached eddies, to link the statistical moments of the filtered wall shear stress fluctuations and the second order structure function of fluctuating velocities at a distance y from the wall. This model suggests that the wall-shear stress fluctuations may induce a higher slope in the turbulence energy spectra of streamwise velocities than the one predicted by the Townsend-Perry attached-eddy model.

* c.diaz-daniel13@imperial.ac.uk

† s.laizet@imperial.ac.uk

‡ j.c.vassilicos@imperial.ac.uk

I. INTRODUCTION

The mean wall shear stress, τ_w, is of obvious importance in turbulent boundary layers and a fundamental variable for their scalings. For fluids with constant density ρ and for sufficiently small wall-normal distances, the mean streamwise velocity profile $\overline{u}$ of a zero-pressure gradient turbulent boundary layer follows a universal "law of the wall" which is typically believed to only depend on the friction velocity $u_\tau = \sqrt{\tau_w/\rho}$ (where τ_w is the mean wall shear stress and ρ is the density of the fluid), the kinematic viscosity ν and the wall-normal distance y [36].

However, the wall shear stress (and the resulting friction velocity) is actually a fluctuating signal and the dynamics of some near-wall mechanisms may not only depend on its mean value τ_w, but also on the statistics of its fluctuations. Even if this has little impact on the non-dimensionalisation of $\overline{u}$, for which the traditional "inner" scaling based only on u_τ and ν may often provide a satisfactory collapse, it nevertheless has profound implications. For instance, the Townsend-Perry attached-eddy model of fluctuating velocities [35, 43] may need to be revisited, since its formulation is only based on the mean friction velocity u_τ with no information about the wall shear stress fluctuations. The intermittency of the shear stress must surely affect the attached-eddy velocity fluctuations and this could modify the structure functions and the power spectra of velocity in the range of wave-numbers associated with the attached eddies.

While the mean skin friction coefficient has been measured experimentally for many years and its Reynolds number dependence is well documented [6, 33], there has been much less attention on the statistics and dynamics of the wall shear stress fluctuations. Only during the last few decades, experiments and, later, numerical simulations have been able to measure the instantaneous wall shear stress with enough temporal and spatial resolution. However, an accurate estimation of the wall shear stress fluctuations is very important, as they are main agents, for instance, in noise radiation, structural vibration, drag properties and wall heat transfer mechanisms.

Early experiments [5, 11, 22, 28], measuring the root-mean squared (rms) fluctuations of the streamwise wall shear stress, $\tau_{x,rms}$, led to high discrepancies with values ranging within $0.06 - 0.40\tau_w$. Alfredsson et al. [2] noticed that this large uncertainty was mostly caused by experimental errors, since the dynamic and static response of the hot-film/hot-wire probes

can be different due to the large thermal inertia of the wall. These experiments suggested a consistent value $\tau_{x,rms} = 0.4\tau_w$ and a normalised skewness and flatness equal to 1.0 and 4.8 respectively. The authors also gave a preliminary estimation of the spanwise shear-stress root mean-squared fluctuations (rms), $\tau_{z,rms} \simeq 0.2\tau_w$. Later experimental measurements [13, 30, 32, 34, 39] obtained similar results.

In recent years, numerical simulations of wall bounded flows at moderate Reynolds numbers have confirmed the results obtained in experiments and have given further information about the shear stress. In experiments, the spatial resolution of hot-films and hot-wires decreases as the Reynolds numbers gets higher and this can lead to erroneously estimating that $\tau^+_{x,rms} = \tau_{x,rms}/\tau_w$ decreases when increasing the Reynolds number. However, results from recent Direct Numerical Simulations (DNS) [1, 15, 34] and laser-Doppler anemometry experiments [12] suggest that $\tau^+_{x,rms}$ actually follows an increasing trend with the Reynolds number, which can be fitted by a logarithmic function. A similar trend has also been proposed for the magnitude of the inner peak found in the rms. profiles of the streamwise velocity [14, 40]. Regarding the spanwise shear-stress fluctuations, there is much less discussion in literature. While this quantity is difficult to obtain in experiments, it can be easily extracted from DNS statistics. For channel flow, Hu et al. [15] also found an increasing dependence of the rms fluctuations $\tau_{z,rms}$ on Reynolds number and suggested that the ratio $\tau_{x,rms}/\tau_{z,rms}$ stays bounded between 1.5 and 2.

The dependence of the shear stress fluctuations on the Reynolds number is very important from a fundamental point of view because it evidences a mixed scaling of inner and outer units. Large scale structures, with size associated with the total boundary layer thickness δ, may have a direct influence on shear stress fluctuations at the wall, possibly through the attached-eddy mechanism proposed by Townsend [43]. Recent computational and experimental studies have provided further evidence on the attached-eddy hypothesis. For instance, the numerical investigations of [14] and [40] suggest that the spanwise integral scale of velocities indeed grows linearly for increasing wall-normal distances y, in accordance to the wall-attached eddy theory. [17] simulated the evolution of self-sustaining wall-attached eddies at specific spanwise scales, proportional to y, revealing that their statistical and energy properties are in good agreement with those predicted by Townsend's theory. The numerical investigation of [9] suggest that if the wall-attached eddies, larger than a given scale, are artificially removed, this may lead to an important reduction of the

mean skin friction coefficient. Based on their results, these authors suggest that the wall-attached eddies may not only contribute to the wall-shear stress fluctuations, but also be responsible for a 20-30% of its total mean value at $Re_\tau = 2000$.

The histogram of the fluctuating streamwise shear-stress signal approximately fits a log-normal distribution, which has an increased probability of extreme positive events [15, 34]. The shape of this distribution and the high kurtosis value are evidence that the wall shear stress is a highly intermittent signal. While mixed scaling in a flow quantity does not necessarily imply intermittency in the time signal, if a turbulent flow variable is intermittent, this may indicate mixed scaling. For isotropic turbulence, Kolmogorov [23] proved, under some appropriate hypotheses, that the intermittency of the dissipation rate ε introduces a mixed scaling in the inertial range of the velocity structure function: $\langle (u'(x+r) - u'(x))^2 \rangle \propto r^{2/3} \varepsilon^{-2/3} \, (L/r)^{-a}$, where the operator $\langle \ \rangle$ denotes spatial averaging, u' is the fluctuating velocity component in the x-direction, r is the spatial separation, L is the integral scale and a is a constant associated with the filtered statistics of the dissipation rate. The last term in the expression arises from the intermittency of the turbulence dissipation rate and introduces a mixed scaling whereby the large scales influence the velocity fluctuations throughout the inertial range of scales.

Along the lines of Kolmogorov [23], a similar mechanism could also be present in wall-bounded turbulent flows, since the wall shear stress and velocity fluctuations inside the boundary layer are linked by the wall-attached eddies. The intermittent fluctuations of the wall shear stress could introduce a mixed scaling to the velocity structure function in the attached-eddy range, thereby modifying the shape of these structure functions and their associated energy spectra. All in all, the wall shear stress does not only present a mixed scaling itself, it can also, via its intermittency, introduce a mixed scaling in the fluctuating velocity field too.

In this article, we start by investigating the wall shear stress statistics using a Direct Numerical Simulation (DNS) of a zero pressure-gradient boundary layer. Some extensive computational studies of the fluctuating shear stress, including correlations, histograms and spectra, are available for channel flows [15, 18], but there is little published on space-developing boundary layers except by Örlü and Schlatter [34]. We present here our results on both the streamwise and spanwise components of the shear stress, and compare them with results found in channel flows. In this first part (Section III), we also study the influence

of the outer variables on the wall shear-stress statistics. In the second part (Section IV) we develop a suggestion made by Vassilicos et al. [44] and propose a theoretical model which relates the intermittency of the wall shear-stress fluctuations to the velocity fluctuations away from the wall. We then use our simulation results to assess the validity of this model. Numerical methods are introduced in in Section II and the main conclusions are summarised in Section V.

II. NUMERICAL METHODS AND NOTATION

The full description of the high-order flow solver, Incompact3D[1], can be found in Laizet and Lamballais [24]. Incompact3D uses 6th order finite difference schemes to discretise the incompressible Navier Stokes equations on a Cartesian mesh, with a pseudo-spectral approach to solve the Poisson equation for the pressure. The current simulation's solution was computed with $4097\times513\times256$ cell points inside a numerical box with size $480\delta_0\times40\delta_0\times15\delta_0$, where δ_0 is the boundary layer thickness at the inlet. A laminar Blasius boundary layer is prescribed at the inlet boundary condition in the streamwise direction x, with Reynolds number $Re_\theta = 270$ based on the momentum thickness θ. At the end of the domain, where the local Reynolds number reaches $Re_\theta = 2200$, a convective equation is solved for the outlet boundary condition. In the spanwise direction z, the boundary conditions were set to periodic. The computational domain is stretched in the wall normal direction and the resolution, in wall viscous units (at $Re_\theta = 1470$) is: $\Delta x^+ = 10.2$, $\Delta z^+ = 5.1$ and $\Delta y^+ = 0.42$ at the wall and $\Delta y^+ = 108.8$ at the top of the domain where a homogeneous Neumann condition is imposed to the three velocity components.

Turbulent conditions have been triggered with the tripping method designed by [38], using the optimal parameters described by these authors. The tripping region is located at $x = 10\delta_0$ and occupies the entire spanwise extent. In this region, a random volume forcing is applied to the wall-normal momentum equation in the near-wall region. The authors of [38] suggest that their tripping mechanism can be compared to a physical region with wall roughness, which is typically used in experiments. According to them, the transition region generated by his tripping method can be significantly shorter than those generated by other (maybe more natural) mechanisms, such as Tollmien-Schlichting waves.

[1] Code available at www.incompact3d.com.

The simulation time-step is $\Delta t = 0.0035\delta_0/U_\infty$ ($\Delta t^+ = 0.013$). Mean quantities and statistics were averaged over a period $T = 3000\delta_0/U_\infty$ ($T^+ = 11000$), where δ_0 is the initial boundary layer thickness (defined at the end of this section) and U_∞ is the free-stream velocity. Time series of the three velocity components were collected in a 3-D array of probing positions over a period $T = 1600\delta_0/U_\infty$ ($T^+ = 6000$). To improve statistical convergence, the variables were averaged along the spanwise direction, where the flow is statistically homogeneous. In the current boundary layer simulation, the Reynolds number based on the skin friction velocity and boundary layer thickness, $Re_\tau = u_\tau\delta/\nu$, is related to Re_θ by the expression $Re_\tau = 86.16 + 0.296Re_\theta$ within the range $Re_\theta = 600 - 2000$ ($Re_\tau = 265 - 680$).

The present simulation results have been carefully validated against reference DNS of turbulent boundary layers such as Jimenez et al. [21] and Schlatter and Örlü [37]. The computed budget terms of the turbulence kinetic energy equation in Figure 1(a) compare very well with Schlatter and Örlü [37] at $Re_\theta = 1420$. The residual (computed as $\mathcal{P} + \mathcal{T} - \varepsilon + \nu\nabla^2 k - \mathbf{u}\cdot\nabla k$, where $\mathcal{P}$ is the production term, $\mathcal{T}$ is the turbulence transport term, ε is the turbulence dissipation rate, $\mathbf{u}$ is the fluid mean velocity vector, and k is the turbulence kinetic energy), which quantifies the deviation from statistical convergence and the cumulative error of the different terms, stays under 1 % of the wall dissipation rate over the entire domain.

The mean profiles of streamwise velocity and the root-mean squared fluctuations of streamwise velocity have also been validated against the simulation data of Schlatter and Örlü [37] and Jimenez et al. [21] and are plotted in Figure 1(b).

Regarding the symbol notation, we refer to the velocity components in the streamwise, wall-normal and spanwise directions x, y, z respectively as u, v, w, or as x_i and u_i with $i = 1$ for streamwise, $i = 2$ for wall-normal and $i = 3$ for spanwise directions when using the index notation. The wall shear stress components are defined as $\tau_x = \rho\nu\partial u(t)/\partial y$ and $\tau_z = \rho\nu\partial w(t)/\partial y$. The mean value of τ_x is expressed as τ_w. The fluctuating velocity and wall shear-stress components are respectively written as u', v', w' and τ_x', τ_z', whereas the rms values of the wall shear stress fluctuations are expressed as $\tau_{x,rms}$ and $\tau_{z,rms}$. The inner region scaling is based on the wall-viscous unit $\delta_\nu = \nu/u_\tau$, generally using the plus notation. The outer region scaling is based on the boundary layer thickness δ, defined as the wall-normal distance where the mean streamwise velocity reaches 99% of the free-stream value.

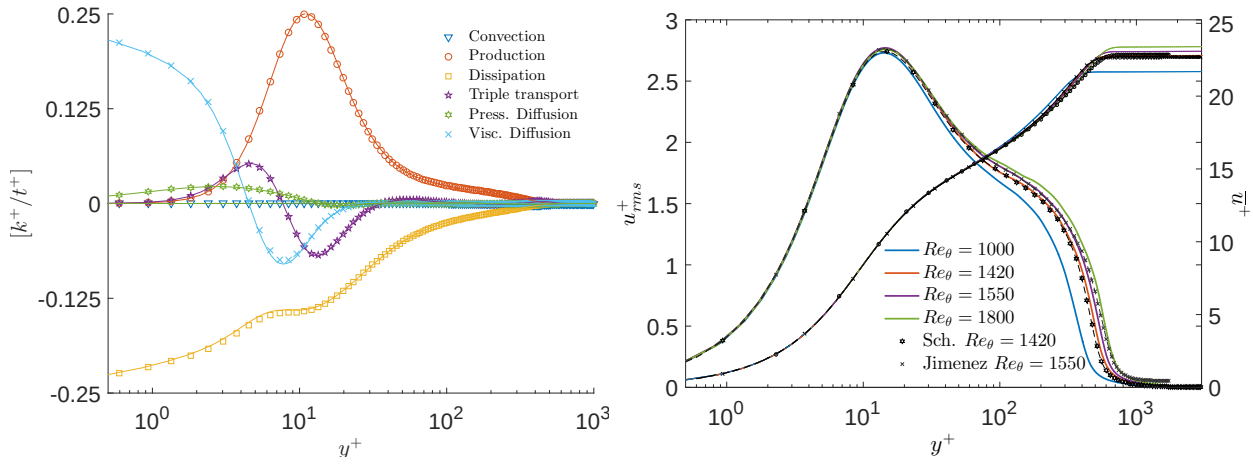

(a) (b)

FIG. 1. (a) Budget terms of the turbulent kinetic energy equation. Current simulation (lines) compared to data from Schlatter and Örlü [37] (symbols). (b) Profiles of mean streamwise velocity and root mean-squared streamwise velocity fluctuations for different Reynolds numbers. Symbols from [37] and [21].

III. RESULTS

A. Statistics for the wall shear-stress fluctuations

The mean friction coefficient $C_f = \tau_w/(0.5\rho U_\infty^2)$, plotted in Figure 2(a) and directly related to the mean skin friction velocity $u_\tau = U_\infty\sqrt{C_f/2}$, has been validated by comparison to well-documented empirical correlations based on extensive experimental data [33], and the error is below 4% for $Re_\theta > 900$. The root mean-squared fluctuations of the streamwise shear stress, shown in Figure 2(b), are in good agreement with the correlation proposed by Örlü and Schlatter [34]:

$$\tau^+_{x,rms} = \tau_{x,rms}/\tau_w = 0.298 + 0.018\ln Re_\tau\,, \tag{1}$$

which is based on previous computational and experimental results and evidences the influence of the outer structures on the inner region. This expression also fits channel data [15] with fair agreement. A relation between Re_θ and Re_τ, used in Figures 2(a) and 2(b), is given in Section II. The peak found in Figure 2(b) is related to the turbulence transition and the tripping method and is also present in the results of Schlatter and Örlü [38]. The

transition effects on this variable do not seem to be of relevance for Reynolds numbers above $Re_\tau = 250$.

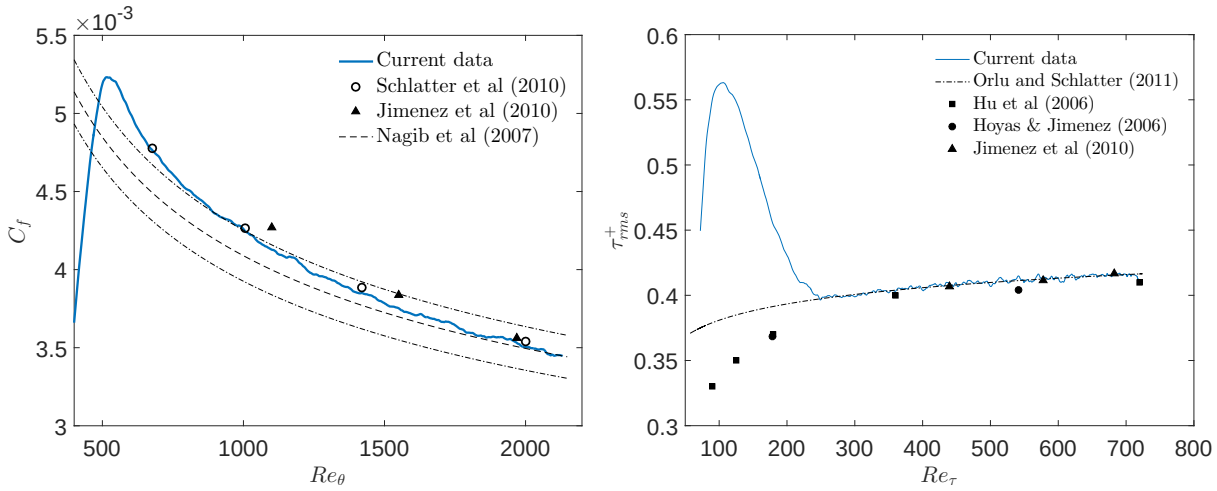

(a) (b)

FIG. 2. (a) Reynolds number dependence of the mean friction coefficient compared against empirical correlations by Nagib et al. [33]. Dashed lines represent an uncertainty of ±4%. (b) Root-mean squared fluctuations of the streamwise wall shear-stress $\tau^+_{x,rms}$ as a function of Reynolds number.

In addition, the current simulation data suggest that the spanwise mean shear-stress fluctuations $\tau^+_{z,rms}$ satisfy a similar logarithmic dependence on the Reynolds number. The only difference between the expressions fitting $\tau^+_{x,rms}$ and $\tau^+_{z,rms}$ seems to be a constant displacement, as seen in Figure 3(a):

$$\tau^+_{z,rms} = 0.164 + 0.018 \ln Re_\tau \,. \tag{2}$$

The dependence of $\tau_{x,rms}$ and $\tau_{z,rms}$ on Reynolds number seen in Figure 3(a) suggests that the influence of the outer motions is similar on $\tau^+_{x,rms}$ and $\tau^+_{z,rms}$, as the curves have the same logarithmic slope. On the other hand, the different constants, 0.298 in Equation ((1)) and 0.164 in Equation ((2)), suggest that the baseline levels of skin friction fluctuations are not the same in the x and z directions, since the near-wall flow field is considerably different for the streamwise and spanwise instantaneous velocity components, u and w respectively.

The expression for the time-averaged turbulence dissipation rate $\overline{\varepsilon} = \nu \overline{\frac{\partial u_i'}{\partial x_j} \frac{\partial u_i'}{\partial x_j}}$ simplifies at the wall, due to the no-slip and incompressibility conditions, to become a function only of the wall shear stress fluctuations: $\overline{\varepsilon}^+ = \left(\tau^+_{z,rms}\right)^2 + \left(\tau^+_{z,rms}\right)^2$ (see book of Pope [36]), where

the plus notation refers to inner variable scaling. It is clear from this relation that the wall shear stress fluctuations could have never been zero. Furthermore, the Reynolds number dependencies ((1)) and ((2)) of the mean squared wall shear-stress fluctuations can be used to write an expression for the mean wall dissipation rate. Figure 3(b) compares this expression with DNS data from turbulent channel and boundary layer flows, and shows that it remains accurate within 5% error, at least for the available moderate Reynolds numbers lower than about $Re_\tau = 4000$. The dispersion of the ε values from the simulation data is higher than the dispersion of $\tau_{x,rms}$ and $\tau_{z,rms}$ because of the square operator in the relation between dissipation and shear stress components. It is important to remark that this dispersion is not related to the previous simplification made to the dissipation expression, which is exact at the wall. An algebraic dependence on Re_τ for the wall dissipation rate can be of relevance to turbulence modelling in order to improve the boundary condition prescription for ε.

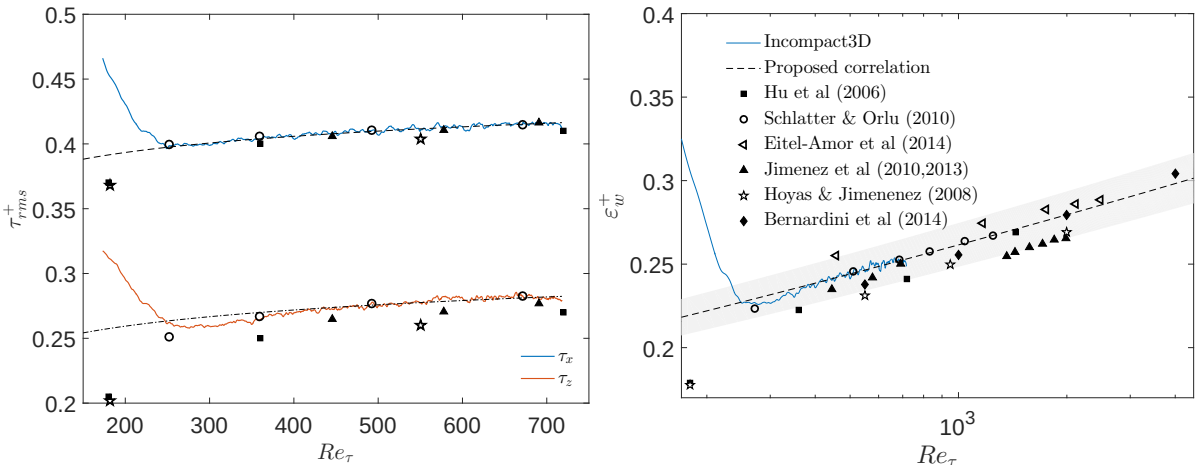

(a) (b)

FIG. 3. (a) Root-mean squared fluctuations of the streamwise and spanwise shear stress at the wall. In dashed lines, correlations in the form $\tau^+_{rms} = C + 0.018 \ln Re_\tau$ where C is 0.298 for τ_x and 0.164 for τ_z. The symbol legend can be found in the right Figure. (b) Dissipation on boundary layers and channels. The shaded area represents an uncertainty of $\pm 5\%$ from the expression $\overline{\varepsilon}^+ = \tau_x'^2 + \tau_z'^2$ using the previous correlations.

The shape of the histograms of the fluctuations of τ_x, τ_z shows important differences between them. While the signal of τ_x is highly (positively) skewed and partly follows a log-normal distribution, the fluctuations of τ_z are not preferentially positive or negative. Alfredsson et al. [3] provide a detailed discussion on the log-normal probability distribution

of τ_x. The kurtosis of τ_z, normalised with the root-mean squared fluctuations, presents high values around $K = 7-8$ (a normal Gaussian distribution has $K = 3$), meaning that extreme events have an increased probability. The numerical value of the statistical moments are included in Table I. The current statistical convergence does not allow to establish a clear dependence of skewness and kurtosis on the Reynolds number. Additionally, the last probe station ($Re_\theta = 1820$) seems to be affected by the outlet, which may lead to an under-prediction of the distribution higher moments.

Re_θ	Re_τ	$S(\tau_x')$	$K(\tau_x')$	$K(\tau_z')$	$\sigma(\psi_\tau)$	$K(\psi_\tau)$	$P(\tau_x < 0)$
1090	409	0.94	4.40	7.20	15.14	13.89	4.71×10^{-4}
1280	465	0.98	4.62	8.29	15.40	18.75	6.21×10^{-4}
1470	521	0.98	4.47	7.10	15.16	14.00	4.02×10^{-4}
1650	574	1.03	4.90	8.94	15.35	17.18	5.28×10^{-4}
1820	625	1.02	4.84	7.99	15.20	13.36	4.38×10^{-4}
[Channel]	$Re_\tau = 720$	1.02	4.97	9.57	-	-	6.23×10^{-4}

TABLE I. Statistical properties of the wall shear-stress components τ_x, τ_z and yaw angle ψ_τ: skewness $S(\cdot)$, kurtosis $K(\cdot)$ and standard deviation $\sigma(\cdot)$. The last row presents results, for comparison purposes, from the channel flow simulation of Hu et al. [15].

The probability distribution function (PDF) of these variables (Figures 4 and 5) suggest that the probability of extreme events becomes higher with increasing Re_θ, as the probability density in the distribution tails becomes higher, in accordance with previous studies. To eliminate the Re_τ effects on the variance, the PDF can be normalised by subtracting the mean and dividing by the rms value (Figures 4(b) and 5(b)). This provides a better collapse of the tails but there is still some dependence on the Reynolds number, especially for the extreme positive events of τ_x, suggesting that the higher moments increase even further with Re_θ.

Insufficient resolution of experimental data has sometimes led to suggest that there are no flow reversals at the wall, $\tau_x < 0$ [8, 46]. However, the present results confirm a small non-zero probability for extreme events where $\tau_x < 0$, in the order of 5×10^{-4}, as shown in Table I, which is consistent with previous numerical studies [15, 25].

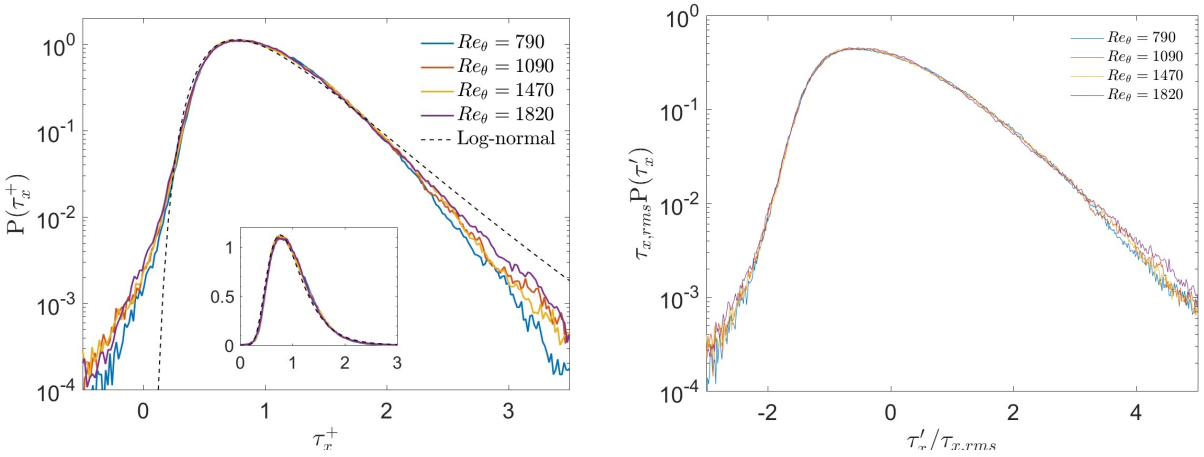

(a) (b)

FIG. 4. (a) Probability distribution function of the streamwise shear-stress for different Reynolds numbers. The PDF of τ_x^+ is compared to a log-normal distribution. (b) PDF of the streamwise shear-stress fluctuations, made non-dimensional using the rms value, which produces a better collapse of the curves.

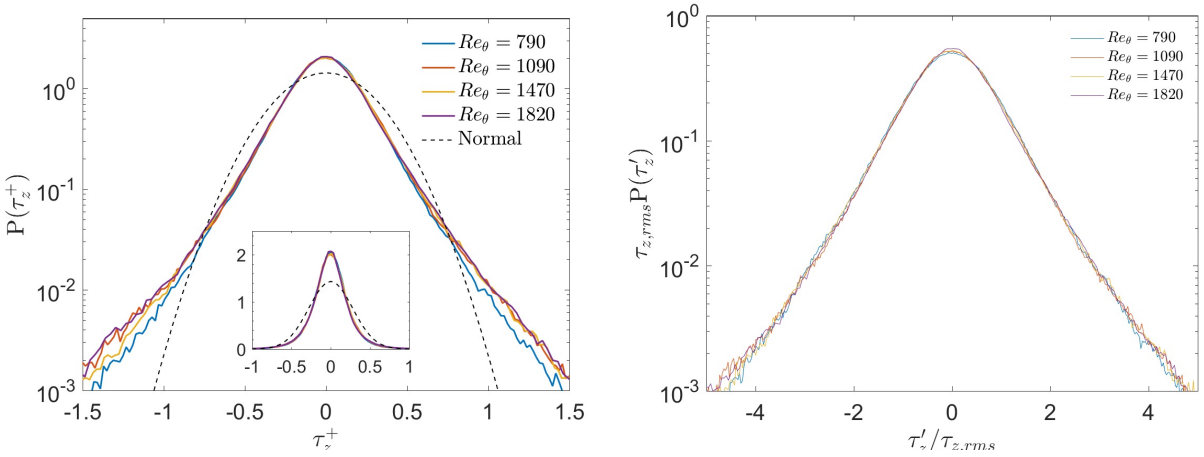

(a) (b)

FIG. 5. (a) Probability distribution function of the spanwise shear-stress for different Reynolds numbers. The PDF of τ_z^+ is compared to a Gaussian distribution. (b) PDF of the spanwise shear-stress fluctuations, made non-dimensional using the rms value, which produces a better collapse of the curves

The relation between the components of the instantaneous shear stress vector $\vec{\tau}(t) = [\tau_x(t), \tau_z(t)]$ can provide an estimation of the yaw angle of the inner layer fluctuations. In

channel flows, Jeon et al. [18] found that events with shear-stress yaw angles outside the range $-45°$ to $45°$ have a very small probability. Indeed, the probability distribution of the shear-stress yaw angle $\psi_\tau(t) = \text{atan}(\tau_z(t)/\tau_x(t))$, shown in Figure 6(a), confirms that the probability of events with angles above 45 degrees is small, below 7×10^{-4} (see Table I). However, the normalised kurtosis of this distribution is very high, around 18, meaning that the wall shear stress signal is dominated by rare events with extreme angle values, explaining the occurrences of $\tau_x < 0$. Since the probability density of $\psi_\tau > 120°$ is much smaller than the probability of $\psi_\tau \approx 90°$, the negative values of the streamwise shear stress fluctuations may be associated with high spanwise fluctuations τ_z. These results are consistent with the findings of [25] in turbulent channel flows.

To further investigate this, Figure 6(b) shows the joint PDF of the vector magnitude and angle of $\vec{\tau}(t) = [\tau_x(t), \tau_z(t)]$, which presents very interesting features. In first place, the probability of events with very low shear-stress magnitude $||\tau||$ is negligible, supporting the view that the zero and negative events of τ_x must be associated with a non-negligible spanwise fluctuation τ_z. Secondly, the relative maximum of the PDF for high values of $|\psi_\tau|$ is related to a value of $||\tau||$ which is close to its mean value. The probability of finding high-magnitude fluctuations is maximum when the shear-stress vector is aligned with the mean flow direction, $|\psi_\tau| = 0$. Recently, a similar analysis on micropillar imaging measurements of the wall-shear stress was performed in [4], which also suggest that the probability of high magnitude events decreases dramatically when the yaw angle is higher than $10 - 20°$. The total probability of backflow events ($|\psi_\tau| > 90°$) reported by these authors, about 0.05%, is in the order of the values found in our DNS (shown in Table I). It is also interesting to compare the analysis presented here for a zero pressure-gradient boundary layer with the results of [45] for a wing section, which presents a strong adverse pressure gradient. These authors suggest that the probability of finding backflow events is much higher in adverse pressure gradient conditions. Moreover, for increasing values of the adverse pressure gradient, their wind rose histograms predict a statistically weaker alignment of the wall shear-stress vector with the streamwise direction.

The yaw angle statistics and the wall dynamics may be related to each other via the turbulence coherent structures found in the inner and buffer regions. The holographic microscopy study of Sheng et al. [39] suggested that the most probable coherent structure occurrences in the near-wall region are pairs of counter rotating streamwise vortices. In our

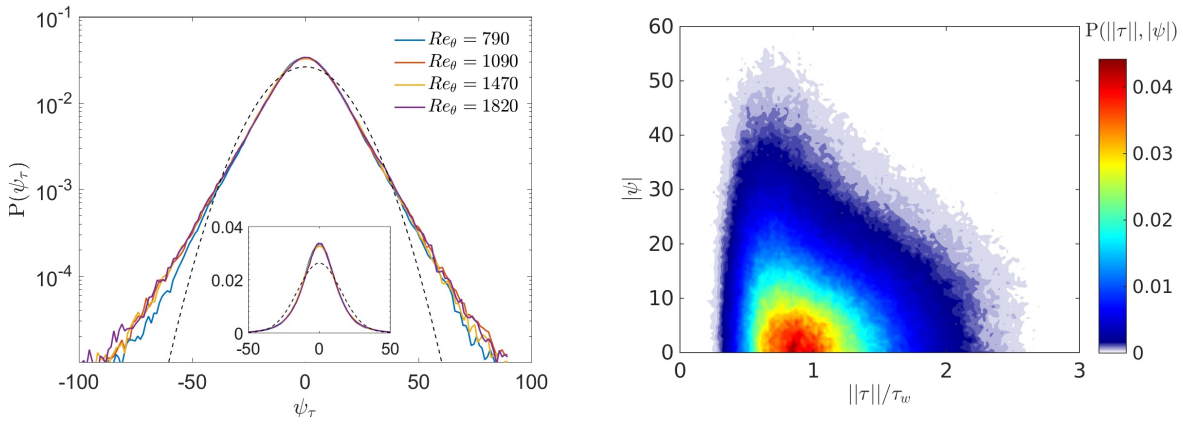

(a) (b)

FIG. 6. (a) Probability distribution of the angle formed between the shear-stress vector and the streamwise direction. The PDF of ψ_τ is compared to a Gaussian distribution for reference. (b) Two-dimensional probability density function of the norm and angle absolute value of the wall shear-stress vector.

simulation, iso-contours of the λ_2 criterion [19], with $\lambda_2^+ = -0.01$ restricted to the region $y^+ < 100$, suggest that this region is mainly populated by streamwise vortices, as shown in Figure 7(a). A streamwise vortex induces velocity fluctuations in the y and z directions and, if the vortex is attached to the wall, this may have an imprint on the spanwise component of the shear-stress. Indeed, Figure 7(a) suggests that the location of vortices might be correlated with regions with high $|\psi_\tau|$. In an arbitrary cross plane $y - z$ at $Re_\theta = 1500$, an example of which is shown in Figure 7(b), the fluctuating velocity field reveals locally high near-wall spanwise velocity fluctuations w' in locations below the centre of attached streamwise vortices. If these passing quasi-streamwise vortices are tilted with respect to the x direction, they can induce small negative fluctuations to the streamwise component of the wall shear-stress. These kind of structures, also suggested by Lenaers et al. [25], may explain the negative events of τ_x and the yaw angle statistics.

We close this section with temporal energy spectra of the wall shear-stress components E_{τ_x}, E_{τ_z}, presented in Figure 8 as functions of the variable $\omega = 2\pi f$, where f is the time frequency. The time resolution is approximately $\Delta t^+ = 0.12$, which gives a maximum Nyquist frequency of $\omega^+_{max} = 26$. In order to improve the statistical convergence of the energy spectra, the time period $T^+ = 6000$ was split and windowed in 16 intervals with

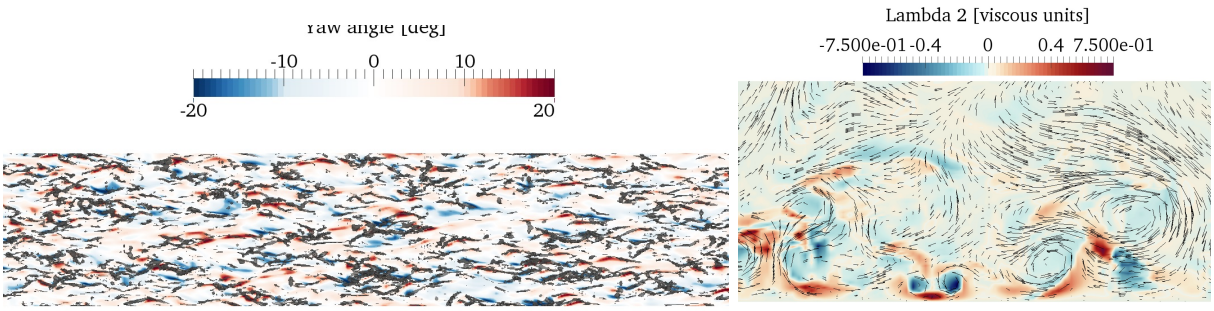

(a) (b)

FIG. 7. (a) Iso-contours of $\lambda_2^+ = -0.01$ in the region $y^+ < 100$ superimposed on contours of the wall shear-stress yaw angle, plotted in the $x - z$ plane, showing good correlation between the structures and regions with high local yaw angle. (b) Contours in a $y - z$ plane of λ_2 against a planar velocity vector field at $Re_\theta = 1500$. One can see that high magnitude of spanwise velocities close to the wall are due to the presence of quasi-streamwise vortices.

50% overlap, which results in a frequency resolution of $\Delta\omega^+ = 8.2 \times 10^{-3}$. Additionally, the energy spectra were computed and averaged over 64 positions in the spanwise direction.

In the curves of shear-stress energy spectra, the medium and high frequency regions are in good collapse for different Reynolds numbers when using inner variables (u_τ and ν), as seen in Figure 8. In the plots, the power spectra have been pre-multiplied by the frequency variable ω to give them squared energy dimensions. Örlü and Schlatter [34] also found that these curves collapse for medium and high frequencies but suggested that the low frequency region contains more energy when the Reynolds number increases. This trend is very slow and, for the limited range of Reynolds numbers covered in our simulations, this dependence is not well captured in Figure 8, due to the limited low frequency resolution of the spectra. The mean statistics were averaged over a longer period and, in particular, the rms fluctuations $\tau_{x,rms}$ and $\tau_{z,rms}$, equal to the integral of the corresponding energy spectra in Figure 8, increase logarithmically with Re_τ, as seen in Figure 3(a). This increasing trend is not manifest in the low frequencies of the energy spectra in Figure 3(a) because the time series which have produced them are shorter by a factor of 2 than the time series that we used to estimate $\tau_{x,rms}$ and $\tau_{z,rms}$. Additionally, the statistics $\tau_{x,rms}$ and $\tau_{z,rms}$ were averaged over all the nodes in the spanwise direction, while we only used 64 temporal probes equally spaced in the z direction to average the energy spectra.

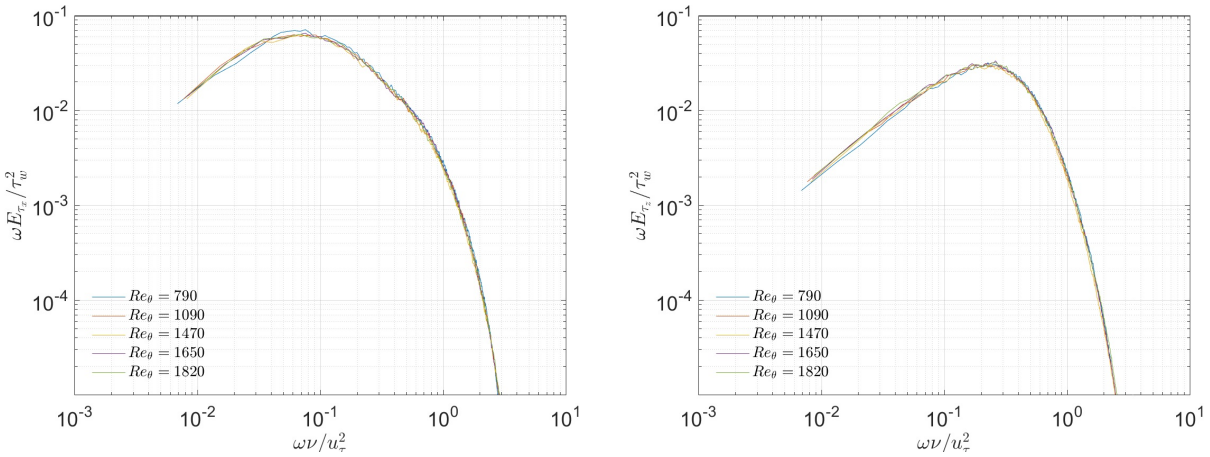

(a) (b)

FIG. 8. Temporal energy spectra of (a) τ_x and (b) τ_z for several Reynolds number.

Hutchins and Marusic [16] suggest that the peak of the premultiplied energy spectra of the streamwise velocity is related to the size of the streamwise streaks which populate the inner region of the boundary layer. Since $E_{11}\omega$ has energy dimensions, the peak frequency ω_{max} may be an indicator of the most energetic turbulence scales, presumably linked to the velocity streaks which dominate the inner region dynamics. The peak frequencies for the spectra of the shear-stress components are $\omega_x^+ = 0.07$, $\omega_z^+ = 0.26$. Using the convection velocity of the streamwise component of the wall shear stress, computed in Appendix A, these peak frequencies can be related to the following streamwise wavelengths $\Lambda = 2\pi U_c/\omega$: $\Lambda_{\tau_x}^+ \approx 1030$, $\Lambda_{\tau_z}^+ \approx 300$ and $\Lambda_{p_w}^+ \approx 240$. As expected, for the streamwise wall shear-stress, the energy-containing scale $\Lambda_{\tau_x}^+$ is much larger than those of the spanwise wall shear-stress and wall pressure. Its value, around 1000 plus units, is consistent with those found in previous studies, as Hutchins and Marusic [16].

IV. MODEL FOR THE VELOCITY FLUCTUATIONS DEPENDENCE WITH THE WALL-SHEAR STRESS

A. Theoretical description

In the previous section, we have investigated the wall shear stress fluctuations and their mixed scaling. Now, the focus of the study is how the intermittency of the wall shear stress

fluctuations may modify the structure function of fluctuating velocities inside the boundary layer and may induce a mixed scaling for the velocity fluctuations due to the attached-eddy mechanism. We propose an analogy with the theoretical study of Kolmogorov [23], who suggested that the dissipation rate fluctuations in free-shear turbulence could affect the inertial range of turbulence energy spectra. In the case of turbulence boundary layers, as suggested in Vassilicos et al. [44], the wall shear stress fluctuations are correlated with the turbulence fluctuations at a distance from the wall by wall-attached eddies, according to Townsend's hypothesis. Therefore, the intermittent fluctuation statistics of the former can be related to the energy spectra of the latter, in the same way that Kolmogorov [23] derived the effect of the dissipation rate's intermittency on the turbulence energy spectra.

The main motivation for this model is to write a simple functional relation which can illustrate how the intermittency of the wall shear-stress can modify the structure function of the velocity fluctuations far away from the wall. Such hypothesis arises from recent observations by Vassilicos et al. [44], who pointed out that the slope of the streamwise energy spectra E_{11} may deviate from the scaling k_1^{-1} predicted by Townsend [43] (where k_1 is the streamwise wavenumber) and may follow a slighlty steeper slope. A model based on the fluctuating wall-shear stress statistics could therefore extend the theory developed by Townsend [43] and Perry et al. [35] and take in account the intermittent flutuations of the wall shear-stress in its formulation. The corrections to the energy spectra predicted by our functional model can complete the modified Townsend-Perry spectra model developed by Vassilicos et al. [44].

According to the Townsend-Perry attached-eddy hypothesis [35, 43], in the wall-normal range $\delta_\nu \ll y \ll \delta$ of the boundary layer, the turbulence energy spectra are dominated by "attached" eddies of wall-normal size r varying in the range $y < r \ll \delta$. If the skin friction is constant, the attached-eddy region of the energy spectra would only depend on u_τ^2 and k_1, so that $E_{11}(k_1, y) \sim u_\tau^2 k_1^{-1}$ for $\frac{1}{\delta} \ll k_1 < \frac{1}{y}$, or an equivalent structure function $\langle (u'(x+r,y) - u'(x,y))^2 \rangle \sim u_\tau^2 \ln(r)$. However, since the shear stress is an intermittent signal, its fluctuation statistics may also appear in the formulation of the energy spectra. Following Kolmogorov [23], to account only for the streamwise scales greater than a given length r, a filtered signal u_*^2 can be defined by applying the following scale-dependent filter to the wall shear stress τ_x/ρ (see Figure 9(a)):

$$u_*^2\,(x,z,r,t) = \frac{1}{2r}\int_{x-r}^{x+r} \nu\,\frac{du(x,z,t)}{dy}\bigg|_{wall} dx\,. \tag{3}$$

In Appendix A, we show that the temporal and spatial scales of the wall shear stress τ_x can be related by a flow convection velocity, $U_c^+ \approx 11$, relatively constant for all wavenumbers. The analysis developed here can therefore be applied indiscriminately to both frequency and streamwise wavenumber spectra for wavenumbers $k_1 \gg 1/\delta$ given that, although the turbulent boundary layer is a spatially developing flow, local homogeneity can be assumed as a good approximation in a region of size similar to δ. The filtering operator defined in Equation (3) for streamwise spatial separations r can also be written in terms of a time filter width $\tau = r/U_c$. Structure functions of velocity can also be formulated in terms of time separations τ which are equal to the spatial separation r divided by the local convection velocity of the streamwise velocity fluctuations. This different convection velocity is approximately equal to the local mean flow velocity at distances higher than $y^+ \approx 40$ from the wall [10].

For filtering times τ or lengths r large enough to neglect the statistical effect of negative wall-shear stress events, the probability distribution function (PDF) of u_*^2 can be assumed to be log-normal, at least for the low-order moments. Therefore, if we define $\xi_r = \ln\left(u_*^2/u_\tau^2\right)$, the PDF of this variable is taken to be:

$$P(\xi_r) = \frac{1}{\sqrt{2\pi}\sigma_r} e^{-(\xi_r-\mu_r)^2/2\sigma_r^2}\,, \tag{4}$$

where μ_r and σ_r are the mean and standard deviation (i.e. rms fluctuations) of the log-normal variable, with $\mu_r = \sigma_r^2/2$ to satisfy the constraint $\langle u_*^2\rangle = u_\tau^2$. For small filter widths, the PDF of the filtered wall shear-stress, shown in Figure 9(b) for $\tau = 0.7\nu/u_\tau^2$, deviates from the log-normal distribution because of the small yet non-negligible presence of negative events. Nevertheless, the negative event contribution becomes smaller as the filter width increases and Figure 9(b) shows that, for sufficiently high filter times, the PDF becomes approximately log-normal, which validates the hypothesis behind Equation (4). Still, the log-normal distribution overestimates the value of the PDF for very high positive events, but these are rare intense events with a combined probability of occurrence that is less than 1% and which therefore has little impact on the lower order moments. Also, the probability of extreme positive events may increase with Re_τ, as suggested in Figure 4, and, thus, the PDF may become more similar to the log-normal distribution for increasing Reynolds numbers.

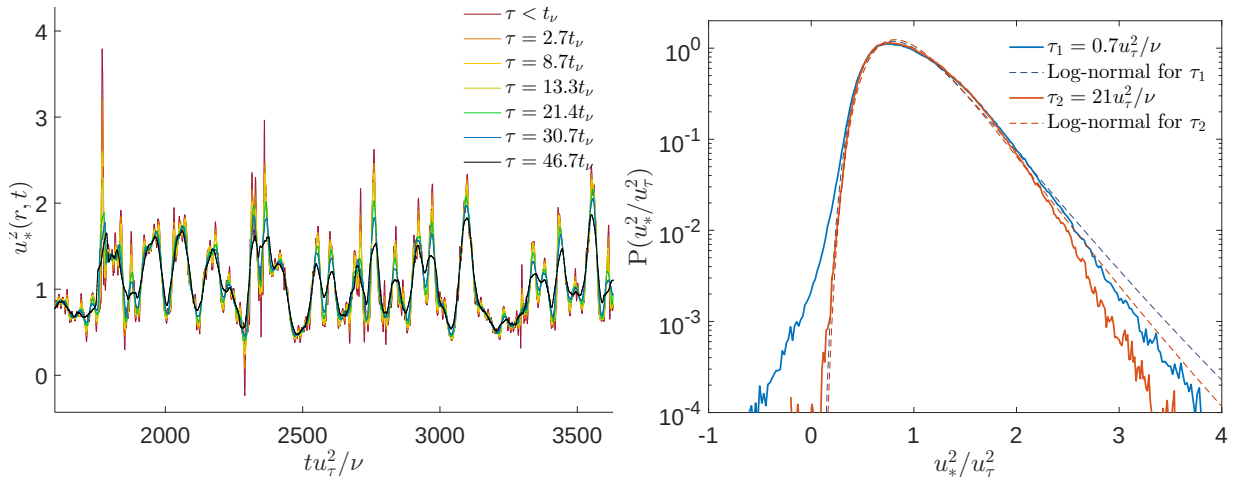

(a) (b)

FIG. 9. (a) Filtered time signal with different filter-width τ for a given x, z, at $Re_\theta = 1420$. The first line $\tau < u_\tau^2/\nu$ represents the unfiltered signal from the simulation. (b) Probability distribution model for the signal at $Re = 1420$ filtered over the time-lengths $\tau = \tau_1 = 7.8\delta_\nu/U_c$ ($\tau_1 = 0.7\nu/u_\tau^2$) and $\tau = \tau_2 = 220\delta_\nu/U_c$ ($\tau_2 = 21\nu/u_\tau^2$). Dotted lines represent the log-normal distributions with the same standard deviation than the previous cases: for τ_1, $\sigma_\tau^2 = 0.152$ and for τ_2, $\sigma_\tau^2 = 0.114$.

Additionally, we can assume, as Kolmogorov [23] did, that the standard deviation σ_r^2 decays logarithmically with the filter width δ/r, i.e. $\sigma_r^2 = A + \mu \ln(\delta/r)$ when the filtering operator is applied in space, or equivalently $\sigma_\tau^2 = A + \mu \ln\left(\frac{\delta}{U_c\tau}\right)$ when it is applied in time. The parameter μ is positive and, by hypothesis, constant for different Reynolds numbers and the parameter A can therefore depend on the macrostructure of the flow [23]. Given that large eddies are attached and therefore feel the wall, A can depend on the Reynolds number Re_τ. The parameters A and μ which fit the DNS curves at each Reynolds number have been obtained by minimising the least-square error in the interval $100 < \tau U_c/\delta_\nu < 1100$. Alternatively, a power-law decay was considered, but the fit of the simulation data was considerably worse.

The optimal value obtained for μ is the same for both Reynolds numbers, suggesting that the hypothesis of constant μ can be accepted as a good approximation. For the available set of data at $Re_\theta = 1090$ and $Re_\theta = 1470$, it turns out that $\sigma_\tau^2 = A + \mu \ln\left(\frac{\delta}{U_c\tau}\right)$ does not collapse our data if A does not vary with Re_τ. For these moderate Reynolds number conditions, if we write $\sigma_\tau^2 = A + \mu \ln(Re_\tau) + \mu \ln\left(\frac{\delta_\nu}{U_c\tau}\right)$, which follows directly from the

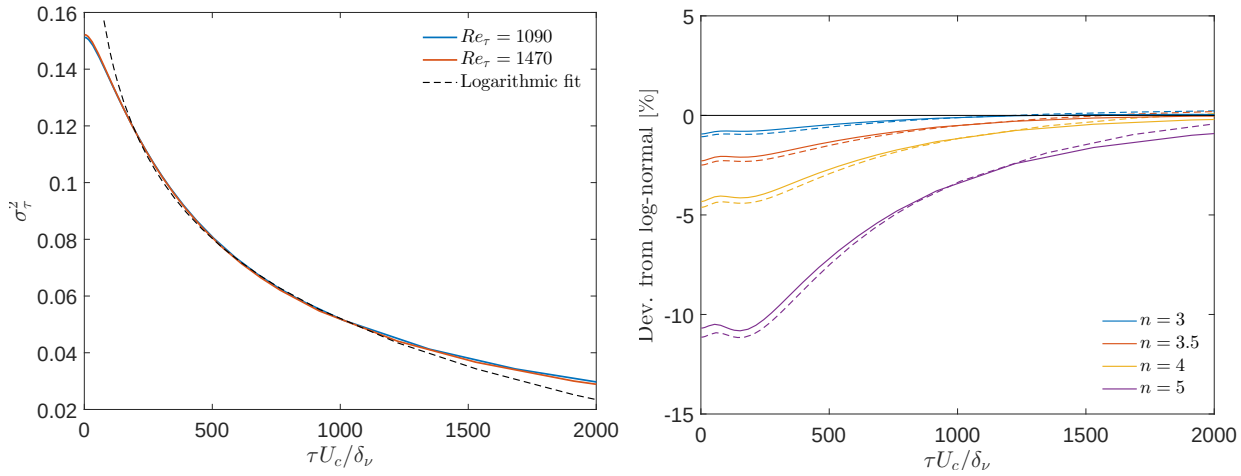

(a) (b)

FIG. 10. (a) Dependence of the variance of the filtered shear stress fluctuations, σ_τ^2, on the filter time-length τ. (b) Deviation between the moment $\langle (u_*^2)^n \rangle$ and the n^{th} raw moment of a log-normal distribution with same σ_τ, for several values of n. Reynolds numbers: $Re_\theta = 1090$ (dashed line) and $Re_\theta = 1470$ (solid line).

previous expression and $\delta/\delta_\nu = Re_\tau$, then the form $\sigma_\tau^2 = A' + \mu \ln\left(\frac{\delta_\nu}{U_c \tau}\right)$ does fit and collapse the data in the range $100 < \frac{\tau U_c}{\delta} < 1100$ with $A' = 0.331$ and $\mu = 0.041$, as seen in Figure 10(a). The relation between A and A' is therefore given by $A = A' - \mu \ln Re_\tau$. For higher Reynolds numbers, the scaling for the parameter A is expected to change, since the current one can predict non-physical negative values of σ_τ^2 for large values of $\tau U_c/\delta_\nu$ if the Reynolds number is sufficiently high. Therefore, the parameter A' may be in general a function of both inner and outer scales, δ_ν and δ and vary away from $A' = 0.331$ at values of Re_θ very different from $Re_\theta = 1090$ and $Re_\theta = 1470$.

The main hypothesis of the current model is a generalisation of the Townsend-Perry attached-eddy hypothesis as follows: the normalised second order structure function of streamwise velocity at a position y, $\langle (u'(x+r,y,t) - u'(x,y,t))^2 \rangle / \langle (u'(x,y,t))^2 \rangle$, is a function of $u_*^2(x,r,t)/u_\tau^2$, at the same separation and filter scale r as long as $y \ll r \ll \delta$.

In the most general way, the non-dimensional structure function $\langle (u'(x+r,y,t) - u'(x,y,t))^2 \rangle / \langle (u'(x,y,t))^2 \rangle$ can be expressed as an arbitrary non-dimensional function of all the statistical moments of the distribution of $u_*^2(x,r,t)$. However, we assume that the low order moments dominate, for which the probability

distribution can be approximately assumed log-normal (up to the 5th moment). Since the moments of a log normal distribution can be related to each other by an analytical algebraic expressions, the non-dimensional function, f, can therefore be simplified to depend on a single moment n:

$$\frac{\left\langle \left(u'(x+r,y,t)-u'(x,y,t)\right)^2\right\rangle}{\left\langle \left(u'(x,y,t)\right)^2\right\rangle} = f\left(\left\langle \left[\frac{u_*^2\,(x,r,t)}{u_\tau^2}\right]^n\right\rangle\right) . \tag{5}$$

The left hand side contains information exclusively on the fluctuating velocity statistics at y and the right hand side is a function of the filtered wall shear-stress fluctuations only. The time-average operation eliminates the time dependence and, if the flow may be considered locally homogeneous in a streamwise distance of the order of δ, then the dependence on x disappears too. For a spatially developing boundary layer, one could argue that the space dependence of the Reynolds number Re_τ is weak compared to the range of interest $y < r \ll \delta$, and the equivalence between time and space averages, using the convection velocity, still holds locally.

Under the assumption of a log-normal distribution for the filtered wall shear-stress, a simple integration provides an exact expression for the nth moment of the distribution. If $\sigma_r^2 = A+\mu\ln(\delta/r)$ as previously suggested, with $A = A'-\mu\ln Re_\tau$ (where A' is approximately a constant), the expression for the moments satisfies the following scaling:

$$\left\langle \left[\frac{u_*^2\,(x,r,t)}{u_\tau^2}\right]^n\right\rangle = \int_{-\infty}^{\infty}\xi^n P(\xi)d\xi = e^{\frac{n(n-1)}{2}\sigma_r^2} \sim (r/\delta)^{-\mu\frac{n(n-1)}{2}} , \tag{6}$$

where the proportionality coefficient depends on the Reynolds number because A is a function of Re_τ. If the function f in equation (5) can be chosen to be a power law with exponent q, which means that one value of n will be best adapted for this, then the resulting expression is:

$$\frac{\left\langle \left(u'(x+r,y,t)-u'(x,y,t)\right)^2\right\rangle}{\left\langle \left(u'(x,y,t)\right)^2\right\rangle} = \beta_s\left(\left\langle \left[\frac{u_*^2\,(x,r,t)}{u_\tau^2}\right]^n\right\rangle\right)^q \sim \left(\frac{r}{\delta}\right)^{-\mu q\frac{n(n-1)}{2}} . \tag{7}$$

This expression can be written in an equivalent way using the temporal filter τ, since the spatial and temporal scales on the left-hand side are related via the convection velocity by $\tau = r/U_c(y)$. This relation for the structure function is different from the relation $\tau = r/U_{c,wall}$ for u_*^2. However, if Equation (6) holds, the difference in the convection velocities only affects the proportionality coefficient in Equation (7) without affecting the power

exponent. Indeed, if the left hand side is written as a function of $\tau = r/U_c(y)$, the value of τ for which the right hand side is evaluated must be scaled with the factor $U_c(y)/U_{c,wall}$. In accordance with Equation (6), this just introduces a new factor $\left(\frac{U_c(y)}{U_{c,wall}}\right)^{-\mu q\frac{n(n-1)}{2}}$ on the right hand side of the equation which can be absorbed in the proportionality coefficient as follows:

$$\frac{\langle (u'(x,y,t+\tau)-u'(x,y,t))^2\rangle}{\langle (u'(x,y,t))^2\rangle} = \beta_t \left(\left\langle \left[\frac{u_*^2(x,\tau,t)}{u_\tau^2}\right]^n \right\rangle\right)^q \sim \tau^{-\mu q\frac{n(n-1)}{2}}, \tag{8}$$

where $\beta_t = \beta_s \left(\frac{U_c(y)}{U_{c,wall}}\right)^{-\mu q\frac{n(n-1)}{2}}$. In Equation (8), the filtering operator in the definition of u_*^2 (see Equation (3)) is now applied in time, with time filter width τ. The factor $U_c(y)/U_{c,wall}$ is always higher than 1 and reaches a maximum value of $U_c(y)/U_{c,wall} \approx 2$ at δ.

Let's assume there exists a particular pair $n = n_{opt}, q = q_{opt}$ which provides the optimal fit for relation (8). According to Equation (7), if the distribution of the filtered shear-stress fluctuations is log-normal, other pairs $n = n^*, q = q^*$ can provide the same optimal prediction as long they satisfy the relation:

$$q^* n^*(n^*-1) = q_{opt} n_{opt}(n_{opt}-1)\,. \tag{9}$$

It is reasonable to choose n to be larger than 1 (which means that q must be strictly negative), as we expect the powerful events to have more of a say than the weak ones. We cannot choose $n = 1$ as $\left\langle \frac{u_*^2}{u_\tau} \right\rangle = 1$ [2], but we can try $n > 1$ and $q < 0$. If the present model holds, the relation between structure function and filtered shear-stress signal would modify the slope in the streamwise energy spectrum in the relevant range of wave-numbers. An inverse relation $q = -1$, with $n > 1$, predicts $E_{11}(k_1, y) \sim k_1^{-1-\mu\frac{n(n-1)}{2}}$ (where $1+\mu\frac{n(n-1)}{2} > 1$) for $\frac{1}{\delta} \ll k_1 \ll \frac{1}{y}$.

Summarizing, our model is a generalisation of the attached-eddy hypothesis in the form of a relation between a particular nth moment of the filtered wall-shear stress fluctuations and the structure function of fluctuating velocity at a position y, where the filter width and the structure function separation length r are equal. Based on simple mathematical assumptions, the model suggests that the shear stress fluctuations may modify the slope of the energy spectrum predicted by the Townsend-Perry theory [35, 43] in the attached-eddy range.

[2] There is a mistake at this point in Section 5 of Vassilicos et al. [44].

B. Validation of the model

The proposed validity range $y < r \ll \delta$ for the model in the previous subsection's analysis needs to take into account the fact that the wall structures are highly anisotropic. It is therefore necessary to find an appropriate way to compare the streamwise separation scale $r = \tau\overline{u}(y)$, and the wall-normal distance y. Figure 11(a) shows the temporal cross-correlation function between fluctuating wall shear-stress and streamwise velocity fluctuations at different y locations and temporal separations τ. The cross-correlation curves were computed using the time-probe signals described in Section II and the results were averaged over time and the spanwise direction. This cross-correlation has a well-defined peak which is located at an increasing time-lag τ for increasing values of y. Figure 11(b) and previous author's data [29, 31] suggest that the time lag of the correlation maximum, τ_{peak}, scales as $y/\bar{u}(y)$. Indeed, the inclination angle $\theta_L = \text{atan}\left[y/\left(\tau_{peak}\bar{u}(y)\right)\right]$ is found to be approximately constant in our simulation, within the range 12-14 degrees, and was estimated to be about 14.1 degrees by Mathis et al. [31]. Although θ_L may or may not represent an actual physical angle of the instantaneous organised motions, the factor $1/\tan(\theta_L)$, in our model, allows to relate wall-normal distance with the streamwise wavenumber or time frequency, revising the attached-eddy range to $\cot(\theta_L)y \ll \tau u(y) \ll \cot(\theta_L)\delta$.

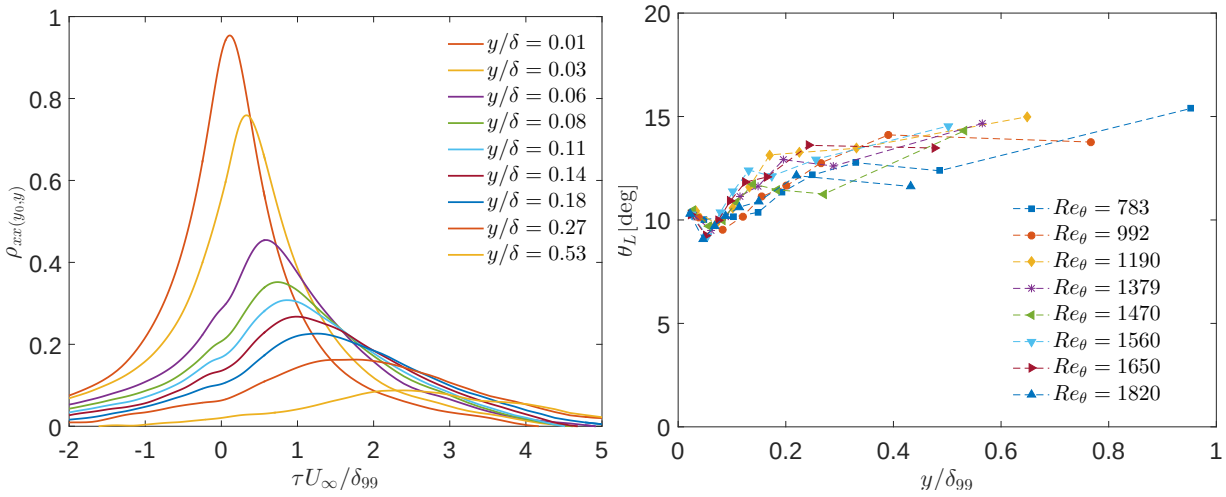

(a) (b)

FIG. 11. (a) Cross-correlation between the shear stress and the streamwise velocity fluctuations at a distance y from the wall in a turbulent boundary layer at $Re_\theta = 1470$. (b) Delay angle $\theta_L = \text{atan}\left(y/\tau_{peak}\overline{u}(y)\right)$ for different heights and Reynolds numbers.

Figure 12 gives evidence that for the straightforward choice $q = -1$ there exists an optimal value of n^* in $1 < n < \infty$ which can produce an approximately constant region for $\left\langle \left[\frac{u_*^2(x,\tau,t)}{u_\tau^2} \right]^n \right\rangle \langle (u'(x,y,t+\tau) - u'(x,y,t))^2 \rangle$, as per Equation (8), over the range $\cot(\theta_L)y < \tau\overline{u}(y) \ll \cot(\theta_L)\delta$. The expected range of validity is indicated in Figure 12 with vertical dotted lines. The lower bound is located at $\tau\overline{u}(y)/y = 4$ since $\cot(\theta_L) \approx 4$ for $\theta_L \approx 14\,\text{deg}$. The validity of the Townsend-Perry hypothesis is expected to fail in the outer region of the flow, which may be assumed to start around $y/\delta \approx 0.3 - 0.4$ [20, 36]. Therefore, the upper bound for the model can be estimated at $\tau\overline{u}(y)/y = 0.4\cot(\theta_L)\delta/y$, which takes different values depending on the y position and Re_τ.

The optimal value of the model coefficient n^* for each y and Re_τ, with fixed $q = -1$, can be computed by finding the best fit for Equation (8) in the range of validity described above. Figure 13(a) shows that the exponent n^* which provides the best fit for the model when using $q = -1$ is always between 3 and 3.5 and that it is reasonably constant for several y positions and the two Reynolds numbers $Re_\theta = 1090$ and $Re_\theta = 1470$. Such values of n for $q = -1$ are very close to the one ($n = 3$) inferred by recent PIV measurements of $E_{11}(k_1)$ [41] and our DNS value $\mu = 0.041$. However, as already mentioned, the statistics of the filtered shear-stress fluctuations are approximately log-normal, at least for the lower moments, meaning that Equation (9) is expected to be satisfied within good approximation. Therefore, for any other value of $q = q^{**} < 0$, the corresponding optimal value of $n = n^{**}$ is approximately related to n^* by $n^{**}(n^{**} - 1) = -n^*(n^* - 1)/q^{**}$ and the model relation (8) would remain equally well satisfied.

The multiplicative factor β_t in Equation (8) remains approximately constant for the available range of y and Re_θ, as seen in Figure 13(b). For the current results, β_t is bounded in the interval $\beta_t \in [2.4, 2.6]$. The highest values found correspond to the positions $y^+ = 150$ (at $Re_\theta = 1090$) and $y^+ = 295$, both locations where $y/\delta > 0.35$ and where the validity of the model may consequently not hold. Otherwise, for all the other cases, the value of β_t was found to be within $\pm 4\%$ of $\beta_t = 2.45$.

In summary, the constant region produced by the curves in Figure 12 suggests that the model works well over the range $1.2\cot(\theta_L)y < \tau u(y) < 0.4\cot(\theta_L)\delta$, consistently with Townsend's wall-attached eddy range. Furthermore, fixing $q^* = -1$, the model parameter n^* in Equation (8) is found to be approximately constant between $3 - 3.5$ for several wall-normal positions and two Reynolds numbers, $Re_\theta = 1090$ and $Re_\theta = 1470$ (see Figure

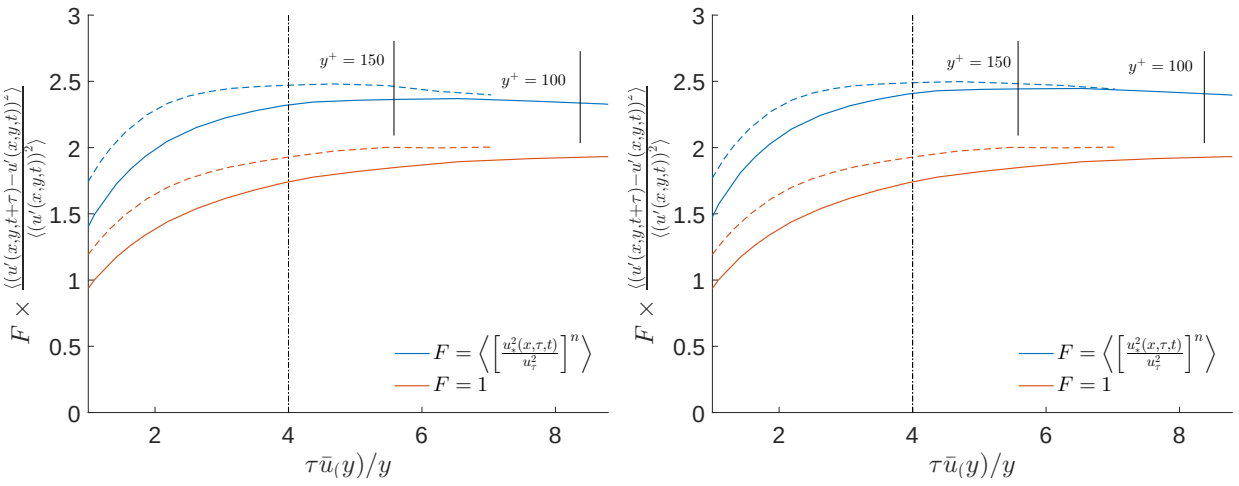

(a) (b)

FIG. 12. Structure function multiplied by $F = 1$ (red) and $F = \left(\left\langle \left[\frac{u_*^2(x,\tau,t)}{u_\tau^2} \right]^n \right\rangle \right)^{-q}$ (blue), with $q = -1$ and optimal n (the optimal value of n is given in Figure 13(a)). Profiles at $y^+ = 100$ (solid line) and $y^+ = 150$ (dotted line), for $Re_\theta = 1090$ (left) and $Re_\theta = 1470$ (right). The constant region shown by the model suggest a validation of the theory in the wall-attached range. Vertical lines bound the region between $\tau = \cot(\theta_L) y/\overline{u}(y) = 4y/\overline{u}(y)$ (- - -) and $\tau = 0.4 \cot(\theta_L)\delta/\overline{u}(y) = 1.6\delta/\overline{u}(y)$(—).

13(a)). Our model implies that the slope of the energy spectra in the wall-attached eddy range is modified by the shear stress fluctuations to $E_{11}(k_1) \sim k_1^{-1+q\mu\frac{n(n-1)}{2}}$. In particular, with $q = -1$ and $n \approx 3$, the model suggests that the energy spectra may take a form close to $E_{11}(k_1) \sim k_1^{-1.12}$. It is not realistic to check this prediction with our DNS data as Re_θ is not sufficiently high to have a clearly defined attached-eddy region in our spectra. However, PIV measurements at much higher values of Re_θ do seem to report such spectra in the log-layer region of turbulent boundary layers [41]. These authors have recently found a wavenumber exponent between -1.1 and -1.2 in the energy spectra of boundary layers with $Re_\theta = 8000 - 20000$.

V. CONCLUSION

In this article, we have studied and extended the mixed scaling of the wall shear-stress fluctuations and we have investigated the relation between filtered wall-shear stress fluctu-

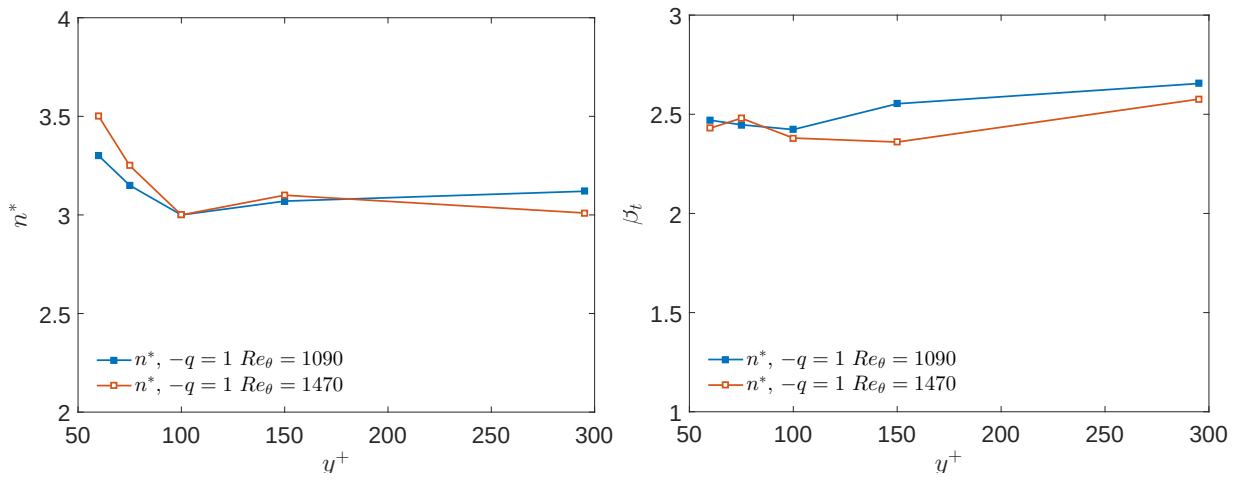

(a) (b)

FIG. 13. (a) Optimum model parameter n for the case $q = -1$. Values computed for different y positions and different Reynolds numbers. (b) Value of the model parameter β_t for different y positions and different Reynolds numbers when using the previous optimal value of n^*.

ations and fluctuating velocities inside the boundary layer. As a result, we have proposed a model which extends the wall-attached eddy theory of Townsend [43] and Perry et al. [35] to take into account the wall shear-stress fluctuations.

The root mean-squared fluctuations of the wall shear-stress streamwise component are in good agreement with the correlation proposed by Örlü and Schlatter [34], $\tau_{x,rms} = 0.245 + 0.018 \ln Re_\tau$. Moreover, the current results do not only support this correlation, but suggest that it can also be extended to the spanwise component as follows: $\tau_{z,rms} = 0.164 + 0.018 \ln Re_\tau$. These estimations can be combined into an explicit correlation for the wall turbulence dissipation rate $\varepsilon_w^+(Re_\tau)$. This correlation has been found to be in good agreement with extensive reference data from both turbulent boundary layers and channel flow. An accurate prediction of ε_w, as a function of Re_τ, may be very useful in some turbulence models which require the specification of wall boundary conditions for the turbulence dissipation rate.

The probability distribution function (PDF) of τ_x and τ_z suggests that the extreme events of the wall shear-stress may have higher probability for increasing Reynolds numbers. Also, the PDF curves collapse better if they are scaled using the standard deviation instead of the mean value. In our DNS dataset, the occurrence of negative events of τ_x has a non-negligible probability which may seem to increase with increasing Re_τ, although the current

data are not sufficient to conclude about this trend. When the streamwise wall-shear stress fluctuations are filtered in time, the probability of negative values of τ_x rapidly decreases for increasing filter times, since these negative values are associated to very extreme events. The PDF of the filtered signal approximates a log-normal distribution in better agreement than the unfiltered one and the variance of the time-filtered wall shear-stress fluctuations decays as a logarithmic function of the filter width τ.

The angle ψ_τ formed between the instantaneous wall shear-stress and the streamwise direction x follows a quasi-normal distribution with high kurtosis. Consequently, it is extremely unlikely to find events with a value of ψ_τ much higher than 90 degrees. This result indicates that the instantaneous negative events of τ_x are essentially associated with high instantaneous values of spanwise wall shear-stress. Vortex visualisations using the negative isocontours of λ_2 and instantaneous velocity vector fields suggest that the high angle events may be related to occurences of quasi-streamwise vortices passing over the wall. If these vortices are tilted with respect to the streamwise orientation, they may induce negative values of τ_x, which could explain the statistical findings.

Finally, a theoretical model following section 5 in Vassilicos et al. [44] was proposed to relate filtered skin friction fluctuations at the wall and fluctuating velocities inside the boundary layer. This study is inspired by the theoretical analysis of Kolmogorov [23]. The theoretical model was initially formulated using spatial correlations and spatial averaging operators. However, the temporal and spatial wall-shear stress fluctuations can be related by defining a convection velocity U_c (see Appendix A), which was found to be approximately constant for all time-separations. This way, the model validation could be performed using time averaging and temporal correlations instead of spatial ones.

The proposed functional model suggests that a particular moment of order $n > 1$ of the distribution of filtered skin friction fluctuations is related to the non-dimensional second order structure function of fluctuating velocities, satisfying $\frac{\langle (u'(x,y,t+\tau)-u'(x,y,t))^2 \rangle}{\langle (u'(x,y,t))^2 \rangle} \sim \left(\left\langle \left[\frac{u_*^2(x,\tau,t)}{u_\tau^2} \right]^n \right\rangle \right)^q$ with $q < 0$ for equal time-filter scales τ and time separations τ. This relation is a good approximation in the range $1.2\cot(\theta_L)y < \tau u(y) < 0.4\cot(\theta_L)\delta$, where $\theta_L \approx 12 - 14^\circ$ is a delay angle which relates the wall-normal and streamwise statistic scales in the near-wall region. The optimal value found for n when $q = -1$ is constant for several y positions and two different Reynolds numbers, $Re_\theta = 1090$ and $Re_\theta = 1470$. For $q = -1$, the optimal values of the parameter n are bounded within the range 3 to 3.5 for all values

of y and Re_θ examined. The proportionality constant in the model relation, $\beta_t \approx 2.45$, is also approximately constant for the different y and Re_τ cases.

As suggested by Vassilicos et al. [44], the influence of the wall-shear stress fluctuations on the fluctuating velocities of the boundary layer via attached-eddies can modify the slope of the turbulence energy spectra. In particular, the results found for our range of $y \sim 100-150$ and $Re_\tau \sim 1000-1500$, with $\mu \approx 0.04$ and $n \approx 0.3$, suggest that the streamwise energy spectra might scale approximately as $E_{11} \sim k_1^{-1.12}$ (instead of -1) in the wall-attached eddy range, where k_1 is the streamwise wavenumber. The slope -1.12, instead of the slope -1 predicted by the theory of Townsend [43] and Perry et al. [35], agrees with recent PIV experiments of turbulent boundary layers by Srinath et al. [41]. This experimental study suggests that the slope of the spectra takes values between -1.1 and -1.2 for $Re_\theta = 8000-20000$. Therefore, the intermittency of the wall shear-stress may indeed effectively modify the energy spectra of the velocity fluctuations in the boundary layer.

ACKNOWLEDGMENTS

This investigation has been funded by the European research project Multisolve, granted by the European Comission (FP7 Marie Curie project, grant agreement No. 317269). The authors would like to aknowledge the use of the following HPC facilities: SuperMUC, thanks to the European research infrastructure PRACE ; ARCHER, supported by the UKTC under the EPSRC grant number EP/L000261/1, and BlueJoule, supported by the STFC Hartree Centre. J.C. Vassilicos acknowledges support from ERC Advanced Grant 320560.

Appendix A: Convection velocity of the wall shear stress

According to the Taylor-hypothesis of frozen-turbulence [26, 27, 42], the spatial and temporal evolution of the turbulent structures are correlated due to the mean-flow convection. This way, the frequency variable ω can be related to a spatial wave-number in the streamwise direction k_x by using a convection velocity $U_c = \omega/k_x$, presumably constant for all wave-numbers and frequencies. Since the velocity at the wall is identically zero, Taylor's hypothesis is not valid in a rigorous sense, and the existence of a convection velocity for the wall shear-stress must be further investigated. The convection velocity can be computed

as the ratio between spatial separations r_x and temporal lapses r_t which maximises the two-dimensional cross-correlation function $\rho(r_x, r_t)$:

$$r_x^* = U_c r_t \quad \longrightarrow \quad \rho(r_x^*, r_t) = \frac{\overline{u'(x + r_x^*, t + r_t)u'(x,t)}}{\overline{u'(x,t)u'(x,t)}} \quad \text{is maximum for a given } r_t \quad \text{(A1)}$$

Alternatively, it can be computed as the ratio between ω and k_x which maximises the power spectral density in the 2-D cross-spectra $E(k_x, \omega)$. DNS data of Del Alamo and Jimenez [10] suggest that, while the convection velocity of the small scales is similar to the mean velocity above $y^+ \approx 10 - 15$, the convection velocity of the big scales is close to the free-stream velocity even in the near-wall region and this results in a non-zero value for the averaged convection velocity at the wall. Jeon et al. [18] and Choi and Moin [7] used space-time autocorrelations and 2-D spectra in a turbulent channel at $Re_\tau = 180$ to confirm the validity of Taylor's hypothesis, and show that τ_x is convected with $U_c = 0.53U_\infty$.

In our DNS simulation, the convection velocity for the streamwise component of the wall shear-stress was computed using Equation A1. The instantaneous value of τ_x was probed at the whole wall plane over a period $T = 1120\delta_{99,0}/U_\infty$, with temporal resolution equal to $\Delta t = 0.35\delta_{99,0}/U_\infty$. The averaging operator defined in Equation A1 can be applied over the total time-period but special caution must be taken when averaging over space, since the boundary layer is a spatially developing flow. The results included here were averaged over time, over the spanwise width and over an interval $x^+ \approx \pm 1000$ around every Reynolds number position. The anal ysis was limited to the region $Re_\theta = 800 - 1800$: lower Reynolds number locations are still affected by the turbulence transition and the statistics of higher Reynolds numbers positions are affected by the outlet. The convection velocity was only computed for the streamwise shear stress component because, in the current simulation, τ_x was the only variable collected simultaneously over time and space in the whole plane $y = 0$. However, Jeon et al. [18] obtained similar convection velocities for the spanwise and streamwise components of the shear-stress: $U_{c,\tau_z} = 0.57U_\infty$ and $U_{c,\tau_x} = 0.53U_\infty$.

Figure 14(a) shows 2-D contours of the space-time autocorrelation at $Re_\theta = 1490$, indicating a clear trend for the maximum position $r_x^{*+}(r_t^+)$. While the maxima are not exactly following a straight line, the hypothesis of constant convection velocity for the wall-shear stress seems to be a good approximation. The convection velocity, defined as $U_c = r_x^*/r_t$ for every r_t, is shown for different Reynolds numbers in Figure 14(b), made non-dimensional

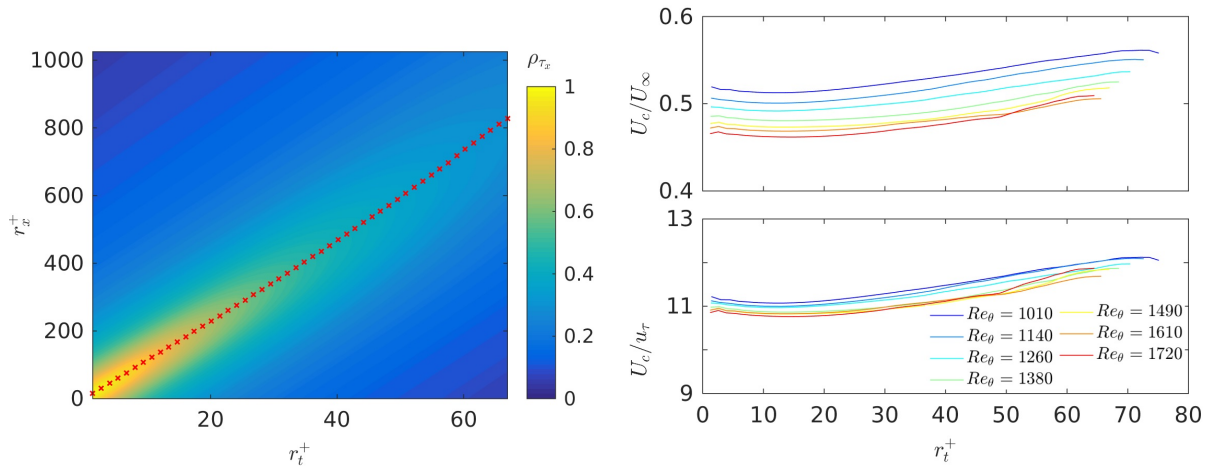

(a) (b)

FIG. 14. (a) 2-D space-time autocorrelation of the streamwise component of the wall-shear stress, at $Re_\theta = 1500$. (b) Convection velocity U_c as a function of the temporal separation r_t, for different Reynolds numbers.

using outer and inner velocities. For all the curves, there is a global minimum at $r_t^+ = 12$ (r_x^+ around 138), which may indicate that, in the inner region, these are the turbulence scales advected at the lowest speed. Above $r_t^+ > 12$, the convection velocity monotonically increases, at least up to $r_t^+ \approx 70 - 80$. This is consistent to the evidence reported by Del Alamo and Jimenez [10], who suggested that the large scales in the inner region were advected with a U_c similar to the free-stream velocity. Figure 14(b) suggests that the collapse of the convection velocity curves for different Reynolds number collapse better using the inner velocity u_τ instead of the free-stream velocity U_∞. However, the collapse is not satisfactory and a clear decreasing trend with the Reynolds number is noticeable. A mean convection velocity can be defined for every Re_θ as the average over all the separation scales, and this averaged convection velocity slowly decreases with Reynolds numbers, approximately as $\overline{U}_c^+ = 12.18 - 5 \times 10^{-4} Re_\theta$ in our limited range of Re_θ.

[1] Abe, H., Kawamura, H., and Choi, H. (2004). Very large-scale structures and their effects on the wall shear-stress fluctuations in a turbulent channel flow up to reτ= 640. *Journal of fluids engineering*, 126(5):835–843.

[2] Alfredsson, P. H., Johansson, A. V., Haritonidis, J. H., and Eckelmann, H. (1988). The fluctuating wall-shear stress and the velocity field in the viscous sublayer. *Physics of Fluids*, 31(5):1026–1033.

[3] Alfredsson, P. H., Örlü, R., and Schlatter, P. (2011). The viscous sublayer revisited–exploiting self-similarity to determine the wall position and friction velocity. *Experiments in Fluids*, 51(1):271–280.

[4] Brücker, C. (2015). Evidence of rare backflow and skin-friction critical points in near-wall turbulence using micropillar imaging. *Physics of Fluids*, 27(3):031705.

[5] Chambers, F. W., Murphy, H. D., and Mceligot, D. M. (1983). Laterally converging flow. part 2. temporal wall shear stress. *Journal of Fluid Mechanics*, 127:403–428.

[6] Chauhan, K. A., Monkewitz, P. A., and Nagib, H. M. (2009). Criteria for assessing experiments in zero pressure gradient boundary layers. *Fluid Dynamics Research*, 41:021404.

[7] Choi, H. and Moin, P. (1990). On the space-time characteristics of wall-pressure fluctuations. *Physics of Fluids*, (2):1450.

[8] Colella, K. and Keith, W. L. (2003). Measurements and scaling of wall shear stress. *Experiments in Fluids*, 34:253.

[9] de Giovanetti, M., Hwang, Y., and Choi, H. (2016). Skin-friction generation by attached eddies in turbulent channel flow. *Journal of Fluid Mechanics*, 808:511–538.

[10] Del Alamo, J. C. and Jimenez, J. (2009). Estimation of turbulent convection velocities and corrections to Taylor's approximation. *Journal of Fluid Mechanics*, 640:5.

[11] Eckelmann, H. (1974). The structure of the viscous sublayer and the adjacent wall region in a turbulent channel flow. *Journal of Fluid Mechanics*, 65(3):439–459.

[12] Fischer, M., Jovanović, J., and Durst, F. (2001). Reynolds number effects in the near-wall region of turbulent channel flows. *Physics of Fluids*, 13(6):1755–1767.

[13] Grosse, S. and Schroder, W. (2009). High reynolds number turbulent wind tunnel boundary layer wall-shear stress sensor. *Journal of Turbulence*, 10:1.

[14] Hoyas, S. and Jimenez, J. (2006). Scaling of the velocity fluctuations in turbulent channels up to Re_τ=2003. *Physics of Fluids*, 18(1):11702.

[15] Hu, Z. W., Morfey, C. L., and Sandham, N. D. (2006). Wall pressure and shear stress spectra from direct numerical simulations of channel flow up to re=1440. *AAIA Journal*, 44(7):1541–1549.

[16] Hutchins, N. and Marusic, I. (2007). Large-scale influences in near-wall turbulence. *Philosophical Transactions of the Royal Society of London A: Mathematical, Physical and Engineering Sciences*, 365(1852):647–664.

[17] Hwang, Y. (2015). Statistical structure of self-sustaining attached eddies in turbulent channel flow. *Journal of Fluid Mechanics*, 767:254–289.

[18] Jeon, S., Choi, H., Yoo, J. Y., and Moin, P. (1999). Space-time characteristics of the wall shear-stress fluctuations in a low-reynolds number channel flow. *Physics of fluids*, 11:3084.

[19] Jeong, J. and Hussain, F. (1995). On the identification of a vortex. *Journal of Fluid Mechanics*, 285:69–94.

[20] Jiménez, J. (2011). Cascades in wall-bounded turbulence. *Annual Review of Fluid Mechanics*, 44(1):27.

[21] Jimenez, J., Hoyas, S., Simens, M. P., and Mizuno, Y. (2010). Turbulent boundary layers and channels at moderate Reynolds numbers. *Journal of Fluid Mechanics*, 657:335–360.

[22] Karlsson, R. I. and Johansson, T. (1986). Ldv measurements of higher order moments of velocity fluctuations in a turbulent boundary layer. In *3rd International Symposium on Applications of Laser Anemometry to Fluid Mechanics*, volume 1, page 12.

[23] Kolmogorov, A. N. (1962). A refinement of previous hypotheses concerning the local structure of turbulence in a viscous incompressible fluid at high reynolds number. *Journal of Fluid Mechanics*, 13(01):82–85.

[24] Laizet, S. and Lamballais, E. (2009). High-order compact schemes for incompressible flows: A simple and efficient method with quasi-spectral accuracy. *Journal of Computational Physics*, 228(16):5989–6015.

[25] Lenaers, P., Li, Q., Brethouwer, G., Schlatter, P., and Örlü, R. (2012). Rare backflow and extreme wall-normal velocity fluctuations in near-wall turbulence. *Physics of Fluids*, 24.

[26] Lin, C. (1953). On Taylor's hypothesis and the acceleration terms in the Navier-Stokes equations. *Quarterly of Applied Mathematics*, 10(4):295–306.

[27] Lumley, J. (1965). Interpretation of time spectra measured in high-intensity shear flows. *Physics of Fluids*, 8(6):1056–1062.

[28] Madavan, N. K., Deutsch, S., and Merkle, C. L. (1985). Measurements of local skin friction in a microbubble-modified turbulent boundary layer. *Journal of Fluid Mechanics*, 156:237–256.

[29] Marusic, I. and Heuer, W. D. C. (2007). Reynolds number invariance of the structure incli-

nation angle in wall turbulence. *Physical Review Letters*, 99:114504.

[30] Marusic, I., Mathis, R., and Hutchins, N. (2011). A wall-shear stress predictive model. *Journal of Physics: Conference Series*, 318:012003.

[31] Mathis, R., Marusic, I., Chernyshenko, S. I., and Hutchins, N. (2013). Estimating wall-shear-stress fluctuations given an outer region input. *Journal of Fluid Mechanics*, 715:163–180.

[32] Miyagi, N., Kimura, M., Shoji, H., Saima, A., Ho, C.-M., Tung, S., and Tai, Y.-C. (2000). Statistical analysis on wall shear stress of turbulent boundary layer in a channel flow using micro-shear stress imager. *International Journal of Heat and Fluid Flow*, 21:576.

[33] Nagib, H. M., Chauhan, K. A., and Monkewitz, P. A. (2007). Approach to an asymptotic state for zero pressure gradient turbulent boundary layers. *Philosophical transactions. Series A, Mathematical, physical, and engineering sciences*, 365:755–770.

[34] Örlü, R. and Schlatter, P. (2011). On the fluctuating wall-shear stress in zero pressure-gradient turbulent boundary layer flows. *Physics of Fluids*, 23:021704.

[35] Perry, A. E., Henbest, S., and Chong, M. S. (1986). A theoretical and experimental study in wall turbulence. *Journal of Fluid Mechanics*, 165:163–199.

[36] Pope, S. (2000). *Turbulent Flows*. Cambridge University Press.

[37] Schlatter, P. and Örlü, R. (2010). Assessment of direct numerical simulation data of turbulent boundary layers. *Journal of Fluid Mechanics*, 659:116–126.

[38] Schlatter, P. and Örlü, R. (2012). Turbulent boundary layers at moderate Reynolds numbers: inflow length and tripping effects. *Journal of Fluid Mechanics*, 710:5–34.

[39] Sheng, J., Malkiel, E., and Katz, J. (2008). Using digital holographic microscopy for simultaneous measurements of 3d near wall velocity and wall shear stress in a turbulent boundary layer. *Experiments in Fluids*, 45(6):1023–1035.

[40] Sillero, J. A., Jimenez, J., and Moser, R. D. (2013). One-point statistics for turbulent wall-bounded flows at Reynolds numbers up to $\delta+ \approx 2000$. *Physics of Fluids*, 25:105102.

[41] Srinath, S., Vassilicos, J. C., Cuvier, C., Laval, J.-P., Stanislas, M., and Foucaut, J.-M. (2017). An attached flow structure model for streamwise energy spectra in a turbulent boundary layer. *Submitted*.

[42] Taylor, G. I. (1938). The spectrum of turbulence. In *Proceedings of the Royal Society of London A: Mathematical, Physical and Engineering Sciences*, volume 164, pages 476–490. The Royal Society.

[43] Townsend, A. A. (1976). *The Structure of Turbulent Shear Flow*. Cambridge University Press, Cambridge.

[44] Vassilicos, J. C., Laval, J. P., Foucaut, J. M., and Stanislas, M. (2015). The streamwise turbulence intensity in the intermediate layer of turbulent pipe flow. *Journal of Fluid Mechanics*, 774:324–341.

[45] Vinuesa, R., Örlü, R., and Schlatter, P. (2017). Characterisation of backflow events over a wing section. *Journal of Turbulence*, 18(2):170–185.

[46] Wietrzak, A. and Lueptow, R. M. (1994). Wall shear stress and velocity in a turbulent axisymmetric boundary layer. *Journal of Fluid Mechanics*, 259:191–218.